Royal Norwegian Council
for Scientific and Industrial Research
(NTNF)

NORSAR

NORSAR Scientific Report No. 1-88/89

Final Technical Summary

1 April – 30 September 1988

L.B. Loughran (ed.)

Kjeller, December 1988

VII.4 The August 8, 1988, Møre Basin earthquake: Observed ground motions and inferred source parameters

An earthquake of magnitude around 5.2 occurred in the Møre Basin on August 8, 1988, with tremors felt over most of southern and central Norway. The earthquake was the largest one in the region for at least 30 years, with a focal mechanism solution that indicates thrust faulting along a NNE-SSW striking fault plane, in response to E-W compressional stress. The seismic moment was of the order of 10^{17} Nm, with indications of a scaling consistent with an ω-square source model. A major source of uncertainty in this analysis is tied to anelastic attenuation.

Background seismicity

The seismicity of this part of Norway and the Norwegian Continental Shelf is shown in Fig. VII.4.1, where three different time periods have been plotted, with different symbols. The map indicates a reasonably good correlation between seismicity and regional geological features such as faults, fault zones, fracture zones and grabens, and there are also indications of the seismicity following the continental margin. The map moreover shows a certain bias between the different time periods in that the areas south of 63°N obviously are better covered in terms of microseismic surveillance during the 1980s (Bungum, 1988).

Epicenter location

The location of the August 8, 1988, earthquake in the Møre Basin is shown in Fig. VII.4.1 at 63.7°N, 2.4°E, slightly west of most earlier events in this area, but still east of the prominent Færøe-Shetland Escarpment. The earthquake was widely recorded on seismic instruments throughout northern Europe and the entire world. Nearly 80 seismic phases have been reported, all within the distance range of 300 to 1300 km. Experiments with locating the event with subsets of these data insured the consistency and reliability of the location. No reliable depth estimate is yet available, however (Hansen et al, 1988).

Felt effects and magnitude

This earthquake was widely felt throughout much of central and southern Norway, along the coast from Stavanger to Mo i Rana, as well as in southeastern Norway and in Sweden. Responses to questionnaires sent out by the Seismological Observatory in Bergen give felt radii of about 300 and 440 km for intensities IV and III, respectively. In using relationships developed recently between felt area and surface wave magnitude M_S (Muir Wood and Woo, 1987), this results in M_S values of 5.2 and 5.3, respectively. In comparison, an M_S value of 5.1 ± 0.24 has been computed by N.N. Ambraseys for this earthquake, while NORESS data have given an M_L value of 5.2. This magnitude makes this earthquake the largest one in the region for at least 30 years, possibly even the largest one since 1895 (Hansen et al, 1988; Bungum and Selnes, 1988).

Focal mechanism

The sense of faulting for this earthquake was explored through the use of the direction of vertical motion of about 50 of the first arriving P-phases for all available recordings. A focal mechanism solution, using this approach, is given in Fig. VII.4.2, where a combination of local and teleseismic data helps in constraining the nodal planes. From the graph, the faulting parameters for the two planes are strike 20°E, dip 46° and rake (slip) 116°, and strike 165°E, dip 50° and rake 66°, respectively. The solution leaves an ambiguity as to which of the two planes is the faulting plane, but in either case this solution gives a reverse mechanism. From the geologic data, however (see Fig. VII.4.1), we find that the preferred fault plane for this earthquake is the one striking 20°E. It can be seen from Fig. VII.4.2 that this northeasterly striking plane is only constrained by the stations whose azimuths vary from about 40° through about 90°. These are the stations of the SEISNOR network and ARCESS. The sense of first motion changed from dilatation to compression through the middle of this network of stations, allowing for a well-constrained fault plane solution (Hansen et al, 1988).

Observed ground motions

An earthquake of magnitude 5.2 naturally causes most conventional seismometers within regional distance ranges to saturate. Unclipped

recordings have, however, in the present case been obtained at three sites: (1) Molde (MOL) accelerometer site within the SEISNOR (Northern Norway) network (288 km); (2) Sulen (SUE) accelerometer site within the Western Norway network (318 km); and (3) NORESS HF (high frequency) and IP (intermediate period) elements (578 km). Since all of these moreover yield broadband recordings, they become especially valuable in terms of inferences about source parameters (NORSAR and Risk Engineering, Inc., 1988).

Observed source displacement spectra for these stations are shown in Fig. VII.4.3, where the time series were rotated to yield the radial (R) and the transverse (T) components. The data are corrected for system response (including a special processing of the accelerometer data), and converted from acceleration to displacement for Molde and Sulen and from velocity to displacement for NORESS (including a careful bandpass filtering in both cases). Energy spectra are then estimated as a basis for the plotted displacements, with a time window covering 24 seconds of the Lg waves.

What is seen from Fig. VII.4.3 is that the observed displacements fall off with frequency at a rate not very different from ω^2 (as indicated by straight lines). At higher frequencies, the slope decreases somewhat, possibly influenced by noise, and at low frequencies it should be kept in mind that the spectra are certainly affected by noise. The filters used in processing these data have been defined at lower cutoffs at 0.20 Hz for Molde (where quantization noise also may have been a problem) and Sulen, at 0.15 Hz for NORESS IP, and at 0.80 Hz for NORESS HF.

Corrected ground motions

In order to be able to compare the observed ground motion displacement spectra more conveniently, we have corrected all of them for the effects of geometrical spreading and anelastic attenuation back to a reference distance of 10 km from the source, with results as shown in Fig. VII.4.4.

The correction used for geometrical spreading has been the commonly used model by Herrmann and Kijko (1983) in which there is a change from spherical to cylindrical spreading at a distance of 100 km:

$$G(R) = \begin{cases} R^{-1} & R < 100 \text{ km} \\ 0.01(R/100)^{-1/2} & R \geq 100 \text{ km} \end{cases}$$

For anelastic attenuation, we have for test and sensitivity purposes used two very different models, by Kvamme and Havskov (1988):

$$Q = 120 \cdot f^{1.1} \qquad \text{(Model 1)}$$

and by Sereno et al (1988):

$$Q = 560 \cdot f^{0.26} \qquad \text{(Model 2)}$$

The first of these has been developed from spectral ratio and coda decay methods based on data typically within a 100-300 km distance range, while the second has been developed from a simultaneous inversion for seismic moment and apparent attenuation based on data between 200 and 1400 km. The first model covers 2-15 Hz, and the second 1-7 Hz.

Even with these differences in mind, it is not obvious which one of the two models will be most appropriate in the present case. With such large differences in frequency sensitivity of the Q-models, however, it is understandable that the effects of the path corrections will be very different, as shown by Fig. VII.4.4. It is useful here to note that if the observed and corrected spectra have slopes proportional to f^{δ} and f^{γ}, respectively, then the following frequency sensitivity of the Q model will be required ($Q = Q_o f^{\eta}$):

$$\eta = 1 - \log\left[1 + \frac{vQ_o(\delta-\gamma)\ln 10}{\pi R}\right]$$

where v is wave velocity and R is distance. This relation shows that if one requires the observed slope to be maintained after corection ($\delta = \gamma$), then Q must be directly proportional to frequency ($\eta = 1$).

From Fig. VII.4.3 it is seen that the observed spectral slopes are reasonably close to ω^2 for most of the data, at least in the 1-5 Hz range. This slope is therefore more or less maintained through the path correction when using the Model 1 attenuation ($\eta = 1.1$) as shown in Fig. VII.4.4, which in turn gives indications of a source model close to the standard ω^2 Brune model (see also Chael and Kromer, 1988). The Model 2 attenuation, on the other side, is more difficult to reconcile with this particular set of data.

Source displacement spectra and seismic moment

From the observed displacement spectra in Fig. VII.4.3 (or from the corrected ones in Fig. VII.4.4), source displacement spectra are obtained simply by correcting all the way back to the source, with the following parameters involved:

$$M_\omega = 4\pi\rho v^3 (S \cdot G \cdot P)^{-1} \Omega_\omega$$

where $P = \exp(\omega R/vQ)$ is anelastic attenuation, G is geometrical spreading as defined above, S is radiation pattern coefficient (0.6) times free-surface amplification (2.0) divided by a possible vectorial partitioning of energy ($\sqrt{2}$), v is wave velocity, ρ is density, and Ω_ω is the observed displacement spectrum. In applying these corrections with a Model 1 attenuation, we get source displacement spectra as shown in Fig. VII.4.5, where a seismic moment of the order of 10^{17} Nm (10^{24} dyne·cm) is indicated. In using the Hanks and Kanamori (1979) moment magnitude relationship

$$M_W = 2/3 \log M_O - 6.0$$

we then get $M_W = 5.3$, which is quite consistent with the other magnitude estimates discussed above. For an earthquake this size, the

Brune source model gives a corner frequency at 0.8 Hz for 100-bar stress drop.

It is not possible from Fig. VII.4.5, however, to determine corner frequency with any reasonable accuracy. The reason for this is partly low frequency noise (as mentioned above), but primarily the fact that the Q-model ($Q = 120 \cdot f^{1.1}$) most probably is not applicable for frequencies below 1 Hz. A lower limit in Q, possibly even combined with an increase towards lower frequencies (Aki, 1980), would yield the low frequency asymptotic effects called for by the commonly accepted source models. The sensitivities and the uncertainties involved here are properly illustrated by the low frequency differences between the two correction models in Fig. VII.4.4: one order of magnitude difference at a distance of about 300 km (Molde, Sulen) and two orders of magnitude differences at about twice that distance (NORESS).

Another question that is raised from the present observations is concerned with the small differences between the Lg amplitudes at Molde/Sulen as compared to NORESS. In the corrected spectra (see Fig. VII.4.5) this shows up in the higher NORESS levels, in spite of the fact that the same time window has been used in the two cases (as compared to using comparable group velocity windows). Since we have not found any technical reasons for this difference (such as errors in gain) we assume that the reason must be tied to Lg wave propagation characteristics that are not being adequately predicted by the models used here.

Concluding remarks

The questions raised here call for continued efforts aimed at resolving existing uncertainties in our knowledge about anelastic attenuation over a wider range of frequencies.

H. Bungum

References

Aki, K. (1980): Attenuation of shear-waves in the lithosphere for frequencies from 0.05 to 25 Hz. Phys. Earth Planet. Inter., 21, 50-60.

Brune, J.N. (1970): Tectonic stress and spectra of seismic shear waves from earthquakes. J. Geophys. Res., 75, 4997-5009. (Correction: J. Geophys. Res., 76, 5002 (1971)).

Bungum, H (1988): Earthquake occurrence and seismotectonics in Norway and surrounding areas. In: S. Gregersen and P. Basham (eds.): Earthquakes at North Sea Passive Margins: Neotectonics and Postglacial Rebound, Kluwer Academic Publ., in press.

Bungum, H. and P.B. Selnes (1988): Earthquake Loading on the Norwegian Continental Shelf - Summary Report. Norwegian Geotechnical Institute and NORSAR, 36 pp.

Chael, E.P. and R.P. Kromer (1988): High-frequency spectral scaling of a main shock/aftershock sequence near the Norwegian coast. Bull. Seism. Soc. Am., 78, 561-570.

Hanks, T. and H. Kanamori (1979): A moment magnitude scale. J. Geophys. Res., 84, 2348-2350.

Hansen, R.A., H. Bungum, L.B. Kvamme, A Dahle and J. Havskov (1988): The 1988 Møre Basin Earthquake. Report for the SEISNOR Steering Committee, 27 pp.

Havskov, J. and H. Bungum (1987): Source parameters for earthquakes in the northern North Sea. Nor. Geol. Tidsskr., 67, 51-58.

Herrmann, R.B. and A. Kijko (1988): Modeling some empirical component Lg relations. Bull. Seism. Soc. Am., 73, 157-171.

Kvamme, L.B. and J. Havskov (1988): Q in southern Norway. Bull. Seism. Soc. Am., in press.

Muir Wood, R. and G. Woo (1987): The Historical Seismicity of the Norwegian Continental Shelf, ELOCS (Earthquake Loading on the Norwegian Continental Shelf) Report 2-1, 117 pp.

NORSAR and Risk Engineering, Inc. (1988): Ground motions from earthquakes on the Norwegian Continental Shelf. Report for Den norske stats oljeselskap a.s., 100 pp.

Sereno, T.S., S.R. Bratt and T. Bache (1988): Simultaneous inversion of regional wave spectra for attenuation and seismic moment in Scandinavia. J. Geophys. Res., 93, 2019-2035.

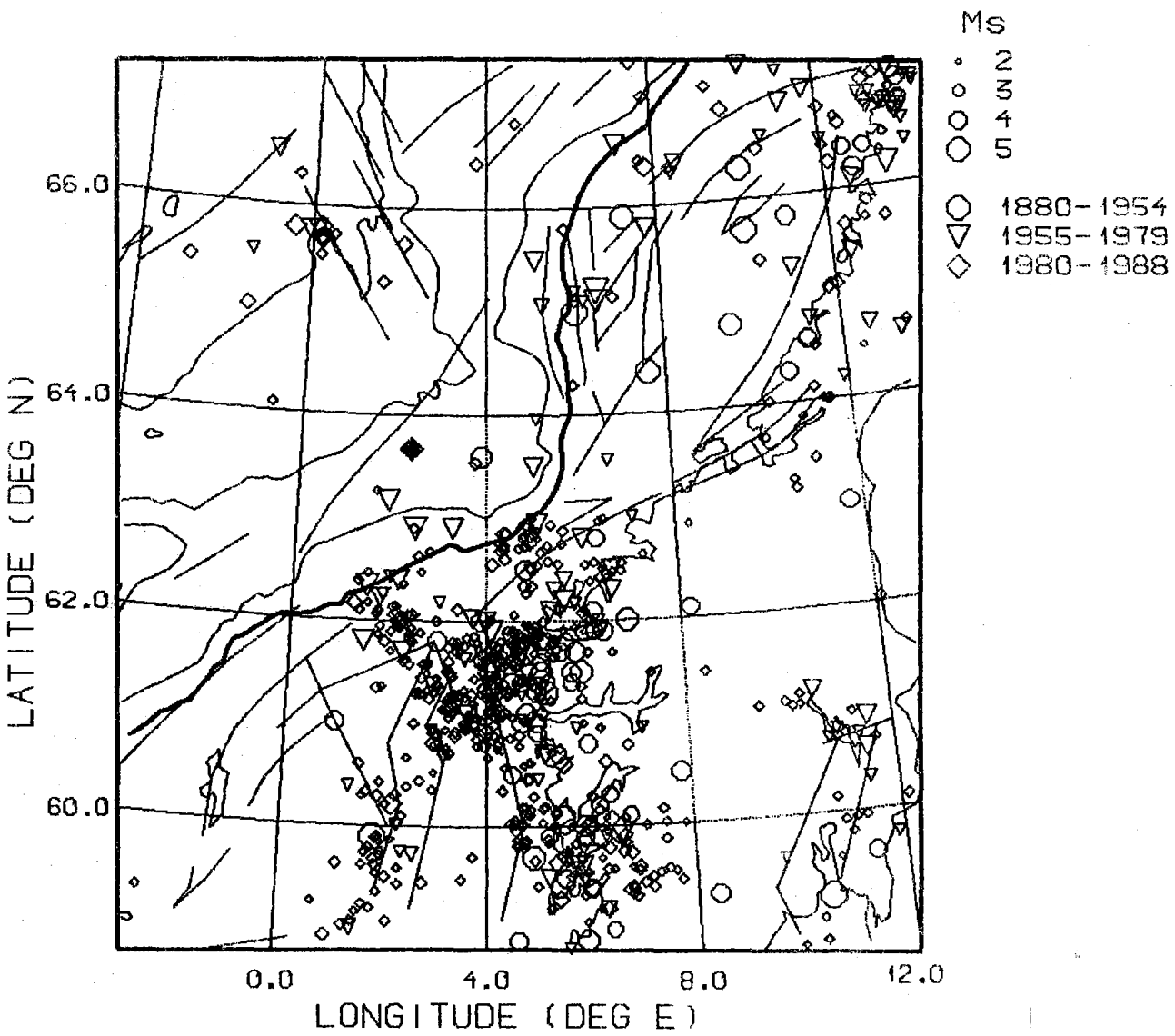

Fig. VII.4.1. Location of the 08.08.88 Møre Basin earthquake (black symbol at 63.7°N, 2.4°E) together with background seismicity for three different time periods, structural information (faults and fracture zones) and bathymetric contours (heavy line is shelf edge).

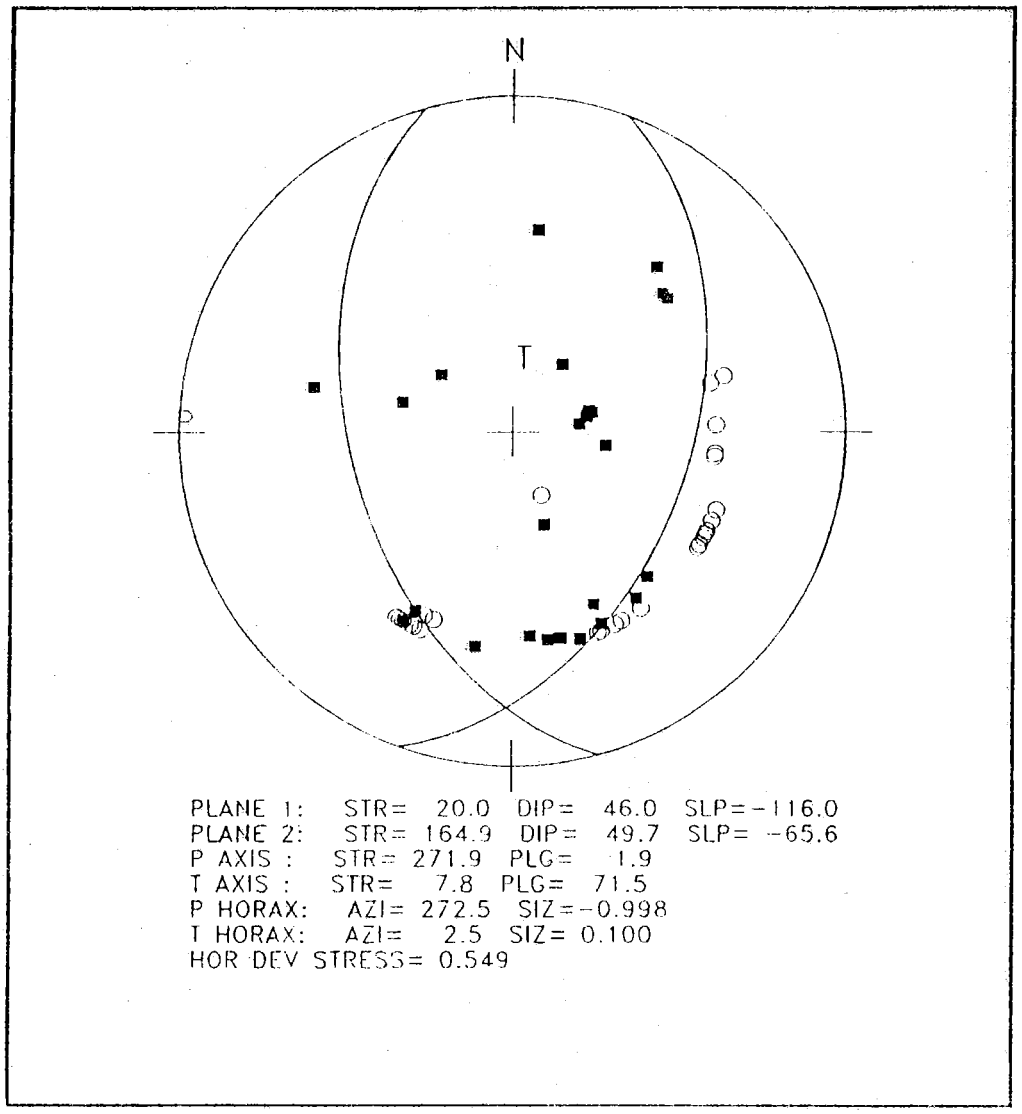

Fig. VII.4.2. Focal mechanism solution (lower hemisphere stereographic projection) for the August 8, 1988, earthquake, based on first motion readings (filled symbols for compressions, open symbols for dilatations) from both local, regional and teleseismic data.
(From Hansen et al, 1988)

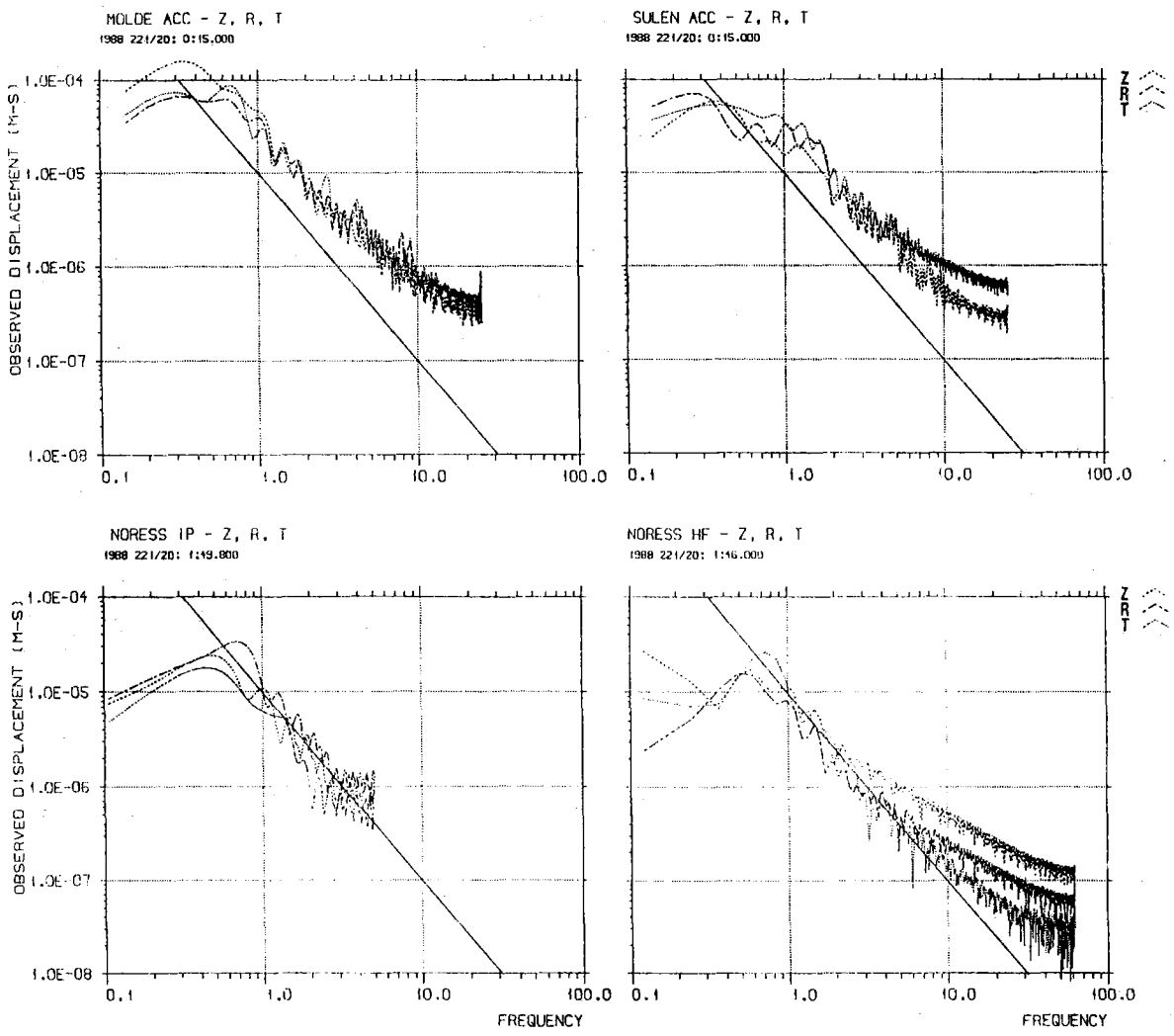

Fig. VII.4.3. Observed ground motion displacement (in m·sec) vs. frequency for Molde (288 km), Sulen (318 km) and NORESS IP and HF (578 km). The data for each station are rotated so as to yield vertical (Z), radial (R) and transverse (T) components. The straight lines correspond to a slope proportional to ω^2.

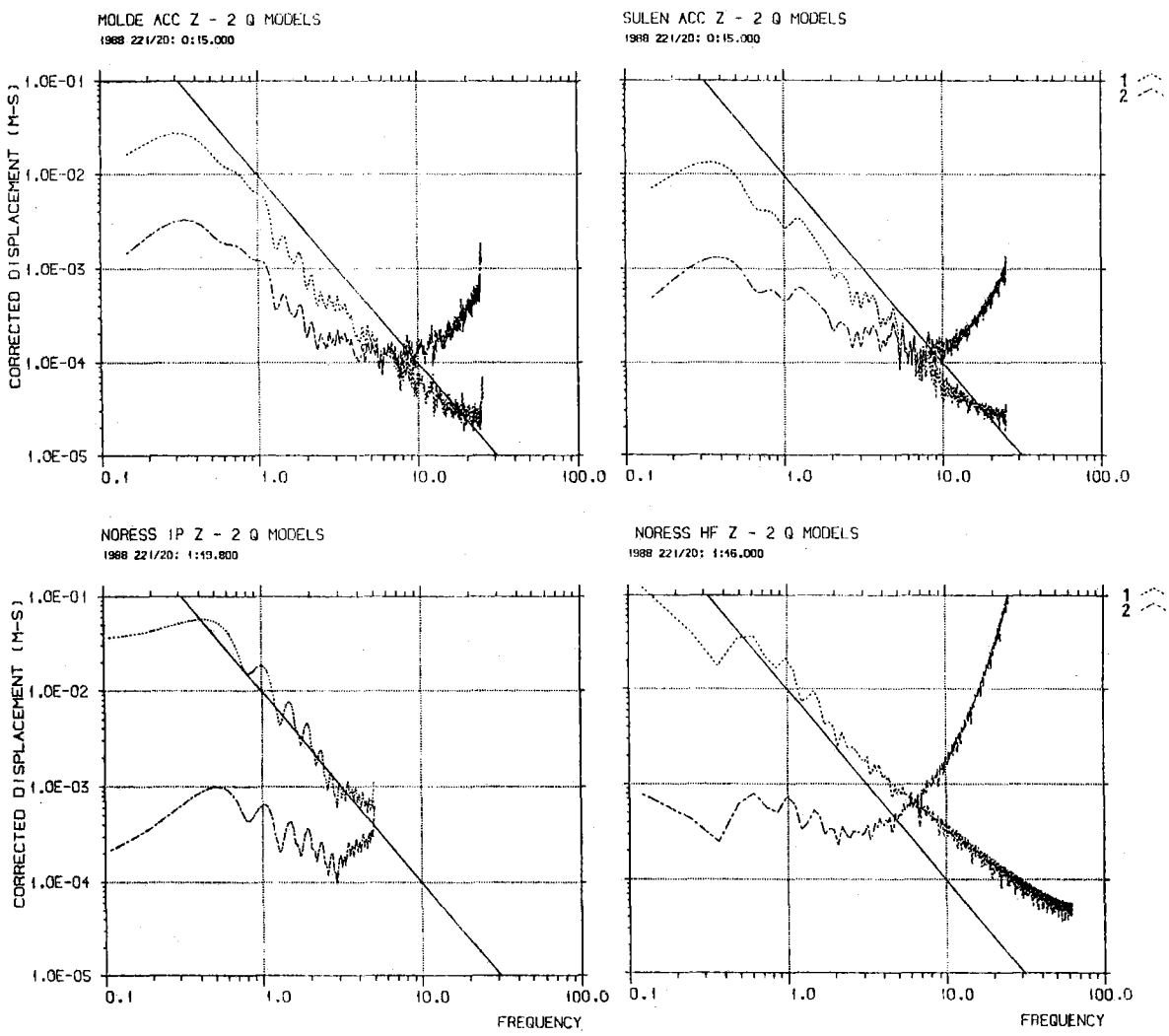

Fig. VII.4.4. Ground motion displacement (in m·sec) vs. frequency for the same data as shown in Fig. VII.4.3 (but for the Z component only), path corrected back to a reference distance of 10 km from the source using the following two Q models: (1) Kvamme and Havskov (1988) and (2) Sereno et al (1988). The straight lines correspond to a slope proportional to ω^2.

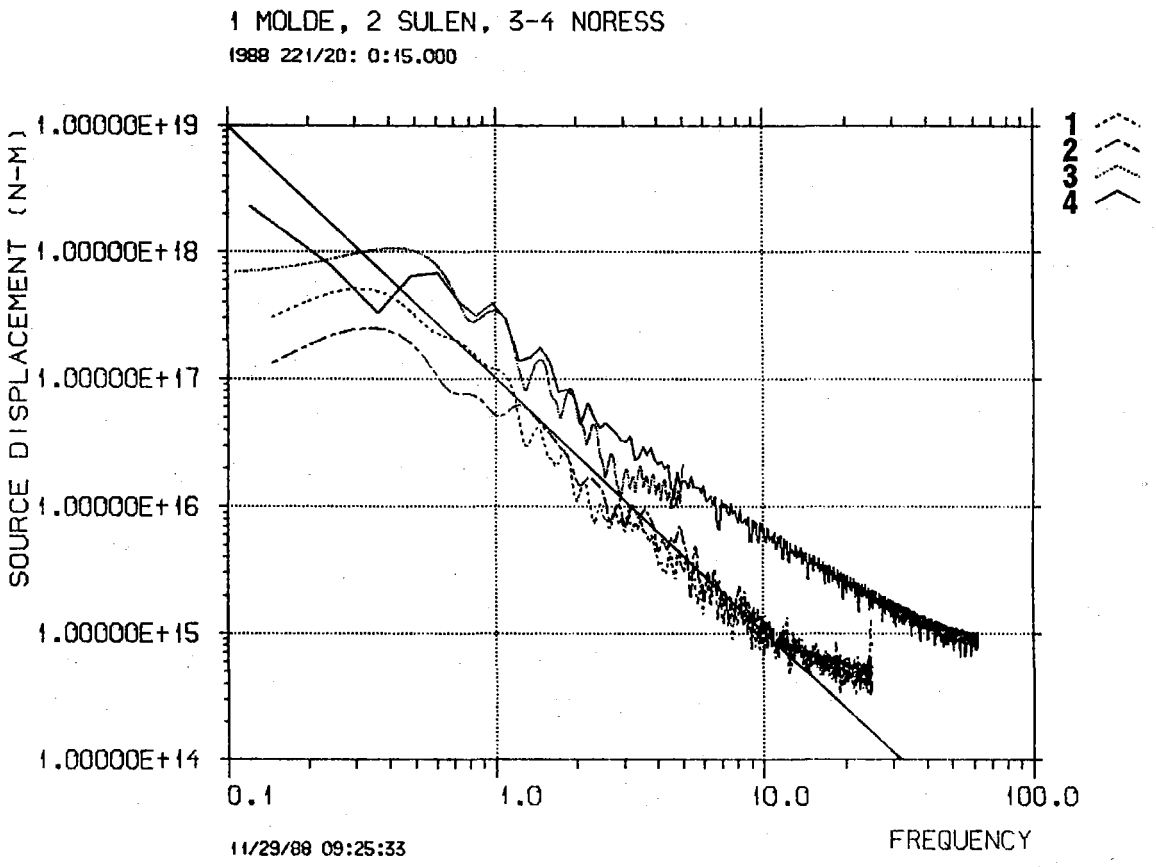

Fig. VII.4.5. Source displacement spectra for the August 8, 1988, earthquake, with corrections for geometrical spreading (Herrmann and Kijko, 1983) and anelastic attenuation (Kvamme and Havskov, 1988). The plot indicates a seismic moment of the order of 10^{17} Newton-meters (equivalent to 10^{24} dyne-cm). The straight line indicates a slope proportional to ω^2, and curves 1 through 4 are Molde, Sulen, NORESS IP and NORESS HF, respectively.